RSC Advances

ROYAL SOCIETY OF CHEMISTRY

www.rsc.org/advances

Na^+ and Zr^{4+} Co-doped $Li_4Ti_5O_{12}$ as Anode Materials with Superior Electrochemical Performance for Lithium Ion Batteries

Peng Lu [a,b], Xiaobing Huang [c,*], Yurong Ren [a,b,d,*], Jianning Ding [a,b,e], Haiyan Wang [f], Shibiao Zhou [c], Yuandao Chen [c], Xiang Ding [c]

[a] School of Materials Science and Engineering, Jiangsu Collaborative Innovation Center of Photovolatic Science and Engineering, Changzhou University, Changzhou 213164, China

[b] Jiangsu Province Cultivation base for State Key Laboratory of Photovoltaic Science and Technology, Changzhou University, Changzhou 213164, China

[c] College of Chemistry and Chemical Engineering, Hunan University of Arts and Science, Changde 415000, China

[d] Jiangnan Graphene Research Institute, Changzhou 213164, China

[e] Micro/Nano Science and Technology Center, Jiangsu University, Zhenjiang 212013, China

[f] College of Chemistry and Chemical Engineering, Central South University, Changsha 410083, China

Abstract

Na^+ and Zr^{4+} co-doped lithium titanates with the formula of $Li_{4-x}Na_xTi_{5-x}Zr_xO_{12}$ (x=0, 0.01, 0.03, 0.05, 0.10, 0.15 and 0.20) were successfully synthesized via a solid-state reaction in air. XRD analysis indicates that Na^+ and Zr^{4+} co-doping do not change the spinel structure of $Li_4Ti_5O_{12}$ and the lattice parameter slightly increases with the enhancement of doping amount. The smaller particle size and the larger BET surface areas are obtained for Na^+ and Zr^{4+} co-doped $Li_4Ti_5O_{12}$ samples. The Four-point probe method and electrochemical impedance spectroscopy (EIS) results demonstrate that Na^+ and Zr^{4+} co-doping $Li_4Ti_5O_{12}$ samples possess higher electrical conductivity and smaller charge transfer resistance compared with undoped $Li_4Ti_5O_{12}$, resulting in improved electrochemical performance. Particularly, $Li_{3.97}Na_{0.03}Ti_{4.97}Zr_{0.03}O_{12}$ exhibits the best rate capability and cycling stability. Even at 20 C, it delivers a discharge capacity of 140mAh g^{-1}, and after 100 cycles at 10 C, 97.7% of its initial capacity is retained.

1.Introduction

Among the currently energy storage systems, the lithium-ion battery (LIB) has received intense attention from both the academic community and industry as the power source in hybrid electric vehicles (HEVs), plug-in hybrid electric vehicles (PHEVs), and

* Corresponding authors: Tel: +86 13762681279.
E-mail address: hxb220170@yahoo.com(X.B. Huang), ryrchem@cczu.edu.cn(Y.R. Ren)

full electric vehicles (EVs) due t o the high energy density.[1] As we know, graphite is used as an anode in commercial LIBs, nevertheless, crucial safety concerns exist in connection with graphite anode, which are attributed to its low operating potential. Metallic lithium will easily give rise to dendrites on the surface of the lithium metal because of the low potential, especially at high rates. Therefore, it is important to find advanced materials with an excellent rate and a better safety capability are critical components for the next generation of LIBs.[2, 3]

Spinel lithium titanate ($Li_4Ti_5O_{12}$) has received considerable attention as a potential candidate for lithium-ion batteries due to its high lithium ion insertion potential at around 1.55 V (*vs.* Li/Li^+), and excellent structural and thermodynamic stability during cycling. $Li_4Ti_5O_{12}$ (LTO) can accommodate lithium insertion during discharge, resulting in a structural transition from spinel-LTO to rock-salt phase $Li_7Ti_5O_{12}$ with its zero-strain characteristics.[4, 5]Unfortunately, the low electronic conductivity (ca. 10^{-13} S cm^{-1}) results in the poor electrochemical performance of LTO, preventing them from being commercially used.[6] To overcome the kinetic problems of LTO, researchers have taken various approaches, such as decreasing its particle size,[7] coating it with conductive material and doping it with transition metal non-metal ions (Li^+,[8] Na^+,[9] Mg^{2+},[10] Zn^{2+},[11] Ca^{2+},[12] Al^{3+},[13] Cr^{3+},[14] La^{3+},[15] Zr^{4+},[16] Ru^{4+},[17] V^{5+},[18] Ta^{5+},[19] W^{6+},[20] F^-[21] and Br^-[22] in the Li, Ti or O sites.

In this research, we found that the radius of Na^+ (113 pm) is larger than Li^+ (73 pm) and the radius of Zr^{4+} (80 pm) is larger than Ti^{4+} (60.5 pm).[9, 23] The doping of Na-Zr will enlarge the lattice parameters of the LTO, and enlarged lattice parameters are beneficial for fast lithium-ion transfer resulting in improving the electrochemical performance of LTO. [11]According to the literature, doping ions with the same valence into the corresponding Li and Ti sites can distort its spinel crystal structure to affect its electrochemical performances.[1] At the same time, few kinds of metal ion can greatly improve the electrochemical performance of LTO, which Na and Zr ions are two of them. More importantly, both doping Na^+ in Li site and doping Zr^{4+} in Ti site singly have been proved that the electrochemical performances of LTO can be highly enhanced based on the reports. So we tried Na and Zr co-doped to LTO naturally. Surprisingly, the results of the electrochemical performances have been highly enhanced because of the so-called 'synergic effect'. However, the mechanism of co-doping is not clear until now, and needs more research. Whereas, Na^+ and Zr^{4+} co-doped LTO has not been investigated as far as we know. For comparison, the pristine LTO without doping was also synthesized.

2. Experimental

$Li_{4-x}Na_xTi_{5-x}Zr_xO_{12}$ (x=0, 0.01, 0.03, 0.05, 0.10, 0.15 and 0.20) compounds were prepared by a conventional solid-stat reaction process using Li_2CO_3 (Aladdin, AR), TiO_2 (Aladdin, AR), and CH_3COONa (Aladdin, AR) and $ZrO(NO_3)_2 \cdot xH_2O$ (Aladdin, AR) as raw materials. the quality proportion between agate ball and total sample is 1∶15. The

obtained slurry was dried at 70 °C for 2 hours in a vacuum oven. The as-prepared powder was heated in a muffle furnace at 750 °C for 8 hours to obtain the final LTO.

X-ray diffraction (XRD) data were examined by X-ray diffractometer (DX-2700, Dandong Haoyuan) utilizing a Cu-Kα1 source. Morphological studies were conducted by scanning electron microscope (SEM, JSM-6510LA) and transmission electron microscopy (TEM, JEOL JEM-2100F). X-ray photoelectron spectroscopy (XPS) measurement was performed on a K-Alpha1063 spectrometer. The BET surface area of the samples was detected by nitrogen adsorption–desorption at -196 ˚C using a Builder SSA-4200 apparatus. Four-point probe method (RTS-9, Guangzhou) was employed to measure the electronic conductivity.

Working electrodes were constructed by mixing the active material, Super-P carbon and LA-132 in the weight ratio of 85:10:5. Water was used as solvent. The slurry was cast onto Al foil using the Doctor-Blade technique and dried at 100 ˚C for 10 h in a vacuum oven. Finally, CR2032 coin-type cells were assembled in an argon-filled glove box, using lithium foil as the counter electrode, Celegard 2400 as the separator, and 1 mol/L $LiPF_6$ dissolved in a mixture of EC, DEC, DMC with a volume ratio of 1:1:1 as the electrolyte. Galvanostatic charge and discharge measurements were performed in a potential range of 1-3 V at 25 ^{o}C. The AC impedance data were recorded in the frequency range 10^{-2} Hz to 10^{5} Hz using CHI600E electrochemical station (Shanghai Chenhua).

3. Results and discussion

Fig. 1 presents the XRD patterns of the pristine and Na-Zr co-doped LTO. The diffraction peaks of $Li_{4-x}Na_xTi_{5-x}Zr_xO_{12}$ (x=0, 0.01, 0.03, 0.05, 0.10, 0.15 and 0.20) compounds in Fig.1 coincide with the cubic spinel structure (JCPDS No. 49-0207) without obvious impurity. However, there are few weak peaks corresponding to the impurity phase in the $Li_{4-x}Na_xTi_{5-x}Zr_xO_{12}$(x=0.15 and 0.20) samples(* for ZrO_2 peaks, # for Na_2O peaks), indicating that few Na and Zr ions do not enter the crystal lattice. The reason may be that the great difference of ionic radius between Na and Li, or Zr and Ti. The enlarged peak of (111) planes of the samples in the Fig. 2 shows that the peaks of the Na-Zr co-doped LTO shifted to smaller angles and indicated an enlarged lattice parameter of the LTO according to the Bragg equation and the precise lattice parameters are listed in the Table 1. Clearly, the lattice parameters become larger and larger with the addition of dopants, when x<0.10. The (111) planes do not shift to a lower angels when x>0.10, and the appearance of the impurity phase in XRD can demonstrate that more dopants cannot enter the lattice cell. All the results shows that the addition of CH_3COONa and $ZrO(NO_3)_2 \cdot xH_2O$ cannot hinder the formation of spinel LTO and the Na^+ and Zr^{4+} have successfully entered the lattice of spinel LTO. The enlarged lattice parameters is beneficial for fast lithium-ion transfer without lattice stability damaged.

Table 1 Lattice parameters of $Li_{4-x}Na_xTi_{5-x}Zr_xO_{12}$ (x＝0, 0.01, 0.03 and 0.05) samples

Sample	a/Å	V/Å^3
$Li_4Ti_5O_{12}$	8.3629	584.89
$Li_{3.99}Na_{0.01}Ti_{4.99}Zr_{0.01}O_{12}$	8.3675	585.85
$Li_{3.97}Na_{0.03}Ti_{4.97}Zr_{0.03}O_{12}$	8.3722	586.84
$Li_{3.95}Na_{0.05}Ti_{4.95}Zr_{0.05}O_{12}$	8.3764	587.73
$Li_{3.90}Na_{0.10}Ti_{4.90}Zr_{0.10}O_{12}$	8.3812	588.73
$Li_{3.95}Na_{0.01}Ti_{4.95}Zr_{0.05}O_{12}$	8.3812	588.73
$Li_{3.95}Na_{0.01}Ti_{4.95}Zr_{0.05}O_{12}$	8.3812	588.73

The XPS spectrum of $Li_{3.97}Na_{0.03}Ti_{4.97}Zr_{0.03}O_{12}$ contains the Li1s, Na1s, C1s, O1s and Zr3d peaks (Fig. 3). The carbon peak may be caused by the carbon oxides in the air. No other peaks were detected, indicating the high purity of the Na-Zr co-doped LTO. Specially, one peak centered on 1071.2 eV, and two broad peaks centered on 182.24 and 184.29 eV are well in accordance with the characteristic peaks of Na1s, $Zr3d_{5/2}$ and $Zr3d_{3/2}$ of Zr^{4+} in $Li_{3.97}Na_{0.03}Ti_{4.97}Zr_{0.03}O_{12}$. The characteristic peaks of Li1s, Ti2p and O1s can be found in $Li_{3.97}Na_{0.03}Ti_{4.97}Zr_{0.03}O_{12}$ as well. Combined with XRD results, all the evidence demonstrated that the $Li_{3.97}Na_{0.03}Ti_{4.97}Zr_{0.03}O_{12}$ composite has been synthesized successfully.

Fig. 4 shows the SEM pictures of $Li_{4-x}Na_xTi_{5-x}Zr_xO_{12}$ (x=0, 0.01, 0.03 and 0.05) compounds. It is apparent that the morphologies of four samples are similar. All the samples are well crystallized with a uniform and narrow size distribution in the range of 200-300 nm. BET analysis was carried out to get further information of the specific surface area change caused by the doping process. The corresponding BET surface areas of the $Li_{4-x}Na_xTi_{5-x}Zr_xO_{12}$ (x=0, 0.01, 0.03 and 0.05) are 8.856 $m^2\ g^{-1}$, 10.611 $m^2\ g^{-1}$, 10.863 $m^2\ g^{-1}$ and 10.869 $m^2\ g^{-1}$, respectively. According to the experimental results, the values of the BET have a slight increase, which may be caused by the increase of particle surface roughness or the decrease of the diameter of crystal particle. In fact, the increase of specific surface area can increase the contact areas of LTO and the electrolyte, resulting in the enhancement of electrochemical performance of Na-Zr co-doped LTO.[7, 24]

To investigate the effect of Na-Zr co-doping on the rate performance of the samples, $Li_{4-x}Na_xTi_{5-x}Zr_xO_{12}$ (x=0, 0.01, 0.03 and 0.05) were tested at various charge-discharge current densities from 0.5 C to 20 C between 1 and 3 V. The results are shown in Fig. 5. Clearly, the margins of discharge capacity between $Li_{3.97}Na_{0.03}Ti_{4.97}Zr_{0.03}O_{12}$ and the other samples become more and more obvious with increasing the current densities. For example, at 0.5 C, 5 C and 10 C the discharge capacity of $Li_{3.97}Na_{0.03}Ti_{4.97}Zr_{0.03}O_{12}$ retains 174 mAh g^{-1}, 152.7 mAh g^{-1} and 140.7 mAh g^{-1}, respectively, while those of $Li_4Ti_5O_{12}$, $Li_{3.99}Na_{0.01}Ti_{4.99}Zr_{0.01}O_{12}$ and $Li_{3.95}Na_{0.05}Ti_{4.95}Zr_{0.05}O_{12}$ are 157.6 mAh g^{-1}, 111.5 mAh g^{-1}, 80 mAh g^{-1}; 170.7 mAh g^{-1}, 145.8 mAh g^{-1}, 138.1 mAh g^{-1} and 173.5 mAh g^{-1} 150.9 mAh g^{-1}, 142.5 mAh g^{-1} at the same rates, respectively. These results indicate that the Na-Zr co-doping could improve the capacity and rate capability of the LTO. The above results demonstrate that $Li_{3.97}Na_{0.03}Ti_{4.97}Zr_{0.03}O_{12}$ exhibits the best rate

performance. As evidenced in four-point results, electronic conductivity of the $Li_{4-x}Na_xTi_{5-x}Zr_xO_{12}$ (x=0, 0.01, 0.03 and 0.05) can be improved when the dopants are increased. Furthermore, the larger specific surface area is obtained with the increasing of dopants, providing more active sites for the electrochemical reaction and reducing path for the electron migration naturally.[25] Therefore, $Li_{3.97}Na_{0.03}Ti_{4.97}Zr_{0.03}O_{12}$ exhibits the better rate performance than $Li_4Ti_5O_{12}$, $Li_{3.99}Na_{0.01}Ti_{4.99}Zr_{0.01}O_{12}$ and $Li_{3.95}Na_{0.05}Ti_{4.95}Zr_{0.05}O_{12}$ for its enhancements of electronic and intrinsic ionic conductivity.

Fig. 6 shows the first charge and discharge curves: (A) $Li_4Ti_5O_{12}$ and (B) $Li_{3.97}Na_{0.03}Ti_{4.97}Zr_{0.03}O_{12}$ at different rates. From Fig. 6, it can been observed that the $Li_4Ti_5O_{12}$ and $Li_{3.97}Na_{0.03}Ti_{4.97}Zr_{0.03}O_{12}$ electrodes both have a discharge plateau at about 1.5 V between 1 V and 3 V respectively, which indicates that the discharge specific capacities of the two electrodes are the result of the electrochemical reaction processes. Also, the charge and discharge curves of $Li_{3.97}Na_{0.03}Ti_{4.97}Zr_{0.03}O_{12}$ are similar in shape with that of $Li_4Ti_5O_{12}$, suggesting that Na^+ and Zr^{4+} co-doping did not change the electrochemical reaction process. In addition, the charge plateaus elevate and the discharge plateaus decrease for both samples with current density increasing, suggesting that the higher polarization at high current densities.

Fig. 7 shows the cycling performance of $Li_{4-x}Na_xTi_{5-x}Zr_xO_{12}$ (x=0, 0.01, 0.03 and 0.05) at 10 C. After 100 cycles, the capacity retention ratio of $Li_{4-x}Na_xTi_{5-x}Zr_xO_{12}$ (x=0, 0.01, 0.03 and 0.05) are 89.2%, 96.9%, 97.7% and 96.2%, respectively. As shown in Fig. 7, the charge and discharge efficiency of the $Li_{3.97}Na_{0.03}Ti_{4.97}Zr_{0.03}O_{12}$ is also better than that of others. It can be clearly seen from the results that too low or too high dopants in the samples do not lead to highest discharge capacity and the best cycle performance. Additionally, the electronic conductivity measured by four-point probe method provides evidence for the above results and the parameters obtained are shown in Table 2. The conductivity of co-doped LTO is much higher than that of LTO. Clearly, the more dopants were added, the larger value of electronic conductivity became. The improvement of the cycle performance may partly correspond to the enhancement of the electronic conductivity. However, the more dopants were added, the more conductive the LTO will become. The battery performance was not better, which may be because the dopants may hinder the Li^+ insertion to the lattice of LTO. The above results suggest that LTO by doping Na and Zr elements is favorable to improve the electrical conductivity and ionic conductivity, resulting superior rate properties.

Table 2 Electronic conductivity for $Li_{4-x}Na_xTi_{5-x}Zr_xO_{12}$ (x=0, 0.01, 0.03 and 0.05).

Samples	Electronic conductivity (S cm^{-1})
X=0	9.80×10^{-5}
X=0.01	6.13×10^{-3}
X=0.03	6.23×10^{-3}

X=0.05	6.82×10^{-3}
X=0.10	7.11×10^{-3}
X=0.15	9.07×10^{-3}
X=0.20	1.76×10^{-2}

To understand the improved electrochemical performance of Na-Zr co-doping LTO, electrochemical impedance spectroscopy (EIS) is evaluated, and the typical Nyquist impedance plots are described in Fig. 8. Each spectrum consists of a depressed semicircle at high frequency and a straight line at low frequency. An intercept at the Z'' axis in the high frequency corresponds to the ohmic resistance (Re), which represents the resistance of the electrolyte and electrode. The high frequency semicircle is related to the charge transfer resistance (R_{ct}), while the straight line in the lower frequency is attributed to the lithium-ion diffusion in LTO.[26] All the parameters obtained from EIS are shown in Table 3. As seen from Fig.8 and Table 3, $Li_{3.97}Na_{0.03}Ti_{4.97}Zr_{0.03}O_{12}$ exhibits a much smaller R_{ct} (1002 Ω) than that of bare LTO (1919 Ω). According to previous report, the effect of R_{ct} can be ignored at a low current density, whereas at a high current density, the R_{ct} is mainly responsible for the voltage drop for the kinetics limitation, thereby leading to deterioration in the electrochemical performance.[27] Appropriate amount of Na^+ and Zr^{4+} doped in LTO is favorable for reducing the electrodes polarization, but that a higher amount of doping is disadvantageous. Moreover, the slope in the low frequency region for co-doped LTO is slightly greater than that of LTO, which could demonstrate that lithium ions diffusion can be easier than that in LTO.

The lithium ion diffusion coefficient could be calculated from the low frequency plots according to the following equation[28-30]:

$$D=R^2T^2/2A^2n^4F^4C^2\sigma^2 \quad (1)$$

where R is the gas constant, T is the absolute temperature, A is the surface area of the cathode, n is the number of electrons per molecule during oxidation, F is the Faraday constant, C is the concentration of lithium ion, and σ is the Warburg factor which is relative with Z_{re} [31, 32]:

$$Z_{re}=R_D+R_L+\sigma\omega^{-1/2} \quad (2)$$

Where ω is frequency. The relationships between Z_{re} and the reciprocal square root of frequency in the low frequency are shown in Fig. 9. All the parameters obtained and calculated from EIS are summarized in Table 3. It can be seen from that the D of LTO doped with Na and Zr is larger by 20 times than that without Na and Zr, and $Li_{3.97}Na_{0.03}Ti_{4.97}Zr_{0.03}O_{12}$ exhibits the smaller charge transfer resistance than that of the LTO. It can be confirmed that the decrease of charge transfer resistance is beneficial to the kinetic behaviors during charge/discharge process. This indicates Na and Zr co-doping is favorable to improve the conductivity of LTO, leading to the improved rate performance and cycle performance, and these results correspond with the cycling performance and the polarization shown in the charge-discharge curve.

Table 3 Impedance parameters of $Li_{4-x}Na_xTi_{5-x}Zr_xO_{12}$ (x=0, 0.01, 0.03 and 0.05)

Samples	$R_e(\Omega)$	$R_{ct}(\Omega)$	σ (Ω $s^{-1/2}$)	D (cm^2 s^{-1})
X=0	10.8	1919	2175	$7.88*10^{-15}$
X=0.01	6.2	1528	1269	$2.31*10^{-14}$
X=0.03	4.7	1002	530	$1.33*10^{-13}$
X=0.05	4.9	1122	1089	$3.14*10^{-14}$

Table 4 compares the result of the current study with the rate capabilities taken from the literature for Na-doped LTO and Zr-doped LTO in a potential range of 1-3 V. The electrochemical performance of $Li_{3.97}Na_{0.03}Ti_{4.97}Zr_{0.03}O_{12}$ obtained in this work is considered highly comparable or even much better than those of the others, implying that both of the two doping elements have strong impact on the electrochemical performance of LTO, appropriate Na-Zr doping is an effective method to improve the rate capability and cycling stability of LTO.

Table 4 Comparison of rate performance of the $Li_{4-x}Na_xTi_{5-x}Zr_xO_{12}$ with Na-doped and Zr-doped $Li_4Ti_5O_{12}$

Sample	**Reaction temperature(℃)/Holding time(h)**	**Particle diameter (nm)**	**Charge /discharge current**	**Discharge capacity (mAh g^{-1})**	**reference**
$Li_{3.9}Na_{0.1}Ti_5O_{12}$	850/24	400-600	5C	133 (1~3V)	[9]
$Li_{3.98}Na_{0.01}K_{0.01}Ti_5O_{12}$	800/10	300-400	10C	56 (1~3V)	[33]
$Li_4Ti_{4.9}Zr_{0.1}O_{12}$	800/10	300-400	10C	132 (1~3V)	[25]
$Li_{3.97}Na_{0.03}Ti_{4.97}Zr_{0.03}O_{12}$	750/8	200-300	10C	148.9(1~3V)	**Current study**

4. Conclusions

In summary, cubic spinel $Li_{4-x}Na_xTi_{5-x}Zr_xO_{12}$ (x=0, 0.01, 0.03 and 0.05) samples were successfully synthesized by means of solid phase method. The structure and electrochemical performance of Na-Zr co-doped LTO were investigated. Na-Zr doping does not change the crystal structure of LTO. A certain amount of Mg-Zr doping increases the specific capacity significantly, as well as the rate capability of LTO. The two doping elements contribute to improvement of the electrochemical property of LTO by the this mechanism: The larger Na^+ into Li^+ and the larger Zr^{4+} into Ti^{4+} exaggerate the

lattice parameters of LTO indicating faster electron transfer kinetics. According to the four probe results, the electronic conductivity has been enhanced greatly at the same time. Sample $Li_{3.97}Na_{0.03}Ti_{4.97}Zr_{0.03}O_{12}$, particle size of 200-300 nm in diameter, has the best rate performance with a large capacity of 148.9 mAh g^{-1} at 10 C, while $Li_4Ti_5O_{12}$ only possesses 111.5 mAh g^{-1}, and after 100 cycles at 10 C, 97.7% of its initial capacity is retained. The superior electrochemical performance can be attributed to the exaggeration of lattice parameters indicating faster electron transfer kinetics and reduced charge transfer resistance in the electrode due to the Na^+ and Zr^{4+} co-dopping. This strategy could pave a new way for LTO and other electrode materials to achieve the significant improvement of electrochemical properties.

Acknowledgements

This project was financially supported by the National Nature Science Foundation of China (No. 21576030, 51304077 and 51574090), the Hunan Provincial Natural Science Foundation of China (No. 13JJ4100), the Construct Program of the Key Discipline in Hunan Province of China (Applied Chemistry), the Opening Project of Material Corrosion and Protection Key Laboratory of Sichuan Province of China (2014CL03 and 2014CL15), the State Key Laboratory of Alternate Electrical Power System with Renewable Energy Sources (No. LAPS15001), the Natural Science Foundation of the Jiangsu Higher Education Institutions of China (No. 15KJA150002) and also sponsored by the Priority Academic Program Development of Jiangsu Higher Education Institutions.

References

1. M. Wagemaker, E. R. H. van Eck, A. P. M. Kentgens and F. M. Mulder, *The Journal of Physical Chemistry B*, 2009, **113**, 224-230.
2. P. Kubiak, A. Garcia, M. Womes, L. Aldon, J. Olivier-Fourcade, P.-E. Lippens and J.-C. Jumas, *Journal of Power Sources*, 2003, **119-121**, 626-630.
3. Q. Guo, S. Li, H. Wang, Y. Gao and B. Li, *RSC Adv.*, 2014, **4**, 60327-60333.
4. Y. Zhang, C. Zhang, Y. Lin, D.-B. Xiong, D. Wang, X. Wu and D. He, *Journal of Power Sources*, 2014, **250**, 50-57.
5. D.-D. Han, G.-L. Pan, S. Liu and X.-P. Gao, *RSC Adv.*, 2015, **5**, 92354-92360.
6. S. Nie, C. Li, H. Peng, G. Li and K. Chen, *RSC Adv.*, 2015, **5**, 23278-23282.
7. Y. Shen, J. R. Eltzholtz and B. B. Iversen, *Chemistry of Materials*, 2013, **25**, 5023-5030.
8. M. Wilkening, W. Iwaniak, J. Heine, V. Epp, A. Kleinert, M. Behrens, G. Nuspl, W. Bensch and P. Heitjans, *Physical Chemistry Chemical Physics*, 2007, **9**, 6199.
9. T.-F. Yi, S.-Y. Yang, X.-Y. Li, J.-H. Yao, Y.-R. Zhu and R.-S. Zhu, *Journal of Power Sources*, 2014, **246**, 505-511.
10. S. Ji, J. Zhang, W. Wang, Y. Huang, Z. Feng, Z. Zhang and Z. Tang, *Materials Chemistry and Physics*, 2010, **123**, 510-515.
11. B. Zhang, H. Du, B. Li and F. Kang, *Electrochemical and Solid-State Letters*, 2010, **13**, A36.

12. Q. Zhang, C. Zhang, B. Li, S. Kang, X. Li and Y. Wang, *Electrochimica Acta*, 2013, **98**, 146-152.
13. H. Zhao, Y. Li, Z. Zhu, J. Lin, Z. Tian and R. Wang, *Electrochimica Acta*, 2008, **53**, 7079-7083.
14. Y. K. Sun, D. J. Jung, Y. S. Lee and K. S. Nahm, *Journal of Power Sources*, 2004, **125**, 242-245.
15. Y.-J. Bai, C. Gong, Y.-X. Qi, N. Lun and J. Feng, *Journal of Materials Chemistry*, 2012, **22**, 19054.
16. Z. Wang, Z. Wang, W. Peng, H. Guo and X. Li, *Ceramics International*, 2014, **40**, 10053-10059.
17. C.-Y. Lin, Y.-R. Jhan and J.-G. Duh, *Journal of Alloys and Compounds*, 2011, **509**, 6965-6968.
18. T.-F. Yi, J. Shu, Y.-R. Zhu, X.-D. Zhu, C.-B. Yue, A.-N. Zhou and R.-S. Zhu, *Electrochimica Acta*, 2009, **54**, 7464-7470.
19. J. Wolfenstine and J. L. Allen, *Journal of Power Sources*, 2008, **180**, 582-585.
20. Q. Zhang, H. Lu, H. Zhong, X. Yan, C. Ouyang and L. Zhang, *J. Mater. Chem. A*, 2015, **3**, 13706-13716.
21. S. Huang, Z. Wen, Z. Gu and X. Zhu, *Electrochimica Acta*, 2005, **50**, 4057-4062.
22. Y. Qi, Y. Huang, D. Jia, S.-J. Bao and Z. P. Guo, *Electrochimica Acta*, 2009, **54**, 4772-4776.
23. T.-F. Yi, B. Chen, H.-Y. Shen, R.-S. Zhu, A.-N. Zhou and H.-B. Qiao, *Journal of Alloys and Compounds*, 2013, **558**, 11-17.
24. Y. Ren, P. Lu, X. Huang, J. Ding, H. Wang, S. Zhou, Y. Chen and B. Liu, *RSC Adv.*, 2015, **5**, 55994-56000.
25. X. Li, M. Qu and Z. Yu, *Journal of Alloys and Compounds*, 2009, **487**, L12-L17.
26. J. Wang, Z. Shao and H. Ru, *Ceramics International*, 2014, **40**, 6979-6985.
27. Y. Ren, P. Lu, X. Huang, J. Ding and H. Wang, *RSC Adv.*, 2016, **6**, 49298-49306.
28. F. Li, M. Zeng, J. Li, X. Tong and H. Xu, *RSC Adv.*, 2016, **6**, 26902-26907.
29. X. Huang, Y. You, Y. Ren, H. Wang, Y. Chen, X. Ding, B. Liu, S. Zhou and F. Chu, *Solid State Ionics*, 2015, **278**, 203-208.
30. H.-Y. Wu, M.-H. Hon, C.-Y. Kuan and I.-C. Leu, *RSC Adv.*, 2015, **5**, 35224-35229.
31. B. Li, C. Han, Y.-B. He, C. Yang, H. Du, Q.-H. Yang and F. Kang, *Energy & Environmental Science*, 2012, **5**, 9595.
32. Y. Ren, P. Lu, X. Huang, S. Zhou, Y. Chen, B. Liu, F. Chu and J. Ding, *Solid State Ionics*, 2015, **274**, 83-87.
33. Z. Liu, L. Sun, W. Yang, J. Yang, S. Han, D. Chen, Y. Liu and X. Liu, *Solid State Sciences*, 2015, **44**, 39-44.

Figure captions

Fig. 1. XRD patterns of as-obtained LTO samples

Fig. 2. The enlarged peak of (111) planes of the samples

Fig. 3. XPS survey spectra of $Li_{3.97}Na_{0.03}Ti_{4.97}Zr_{0.03}O_{12}$ (A), typical high-resolution XPS spectra of Na 1s for $Li_{3.97}Na_{0.03}Ti_{4.97}Zr_{0.03}O_{12}$ (B) and typical high-resolution XPS spectra of Zr 3d for $Li_{3.97}Na_{0.03}Ti_{4.97}Zr_{0.03}O_{12}$ (C)

Fig. 4. SEM pictures of $Li_{4-x}Na_xTi_{5-x}Zr_xO_{12}$ samples: (A) x=0, (B) x=0.01, (C) x=0.03, and (D) x=0.05

Fig. 5. Cycling performance of $Li_{4-x}Na_xTi_{5-x}Zr_xO_{12}$ (x=0, 0.01, 0.03 and 0.05) at various rates

Fig. 6. The first charge and discharge curves for $Li_4Ti_5O_{12}$ (A) and $Li_{3.97}Na_{0.03}Ti_{4.97}Zr_{0.03}O_{12}$ (B) at various rates

Fig.7. Cyclic performance of $Li_{4-x}Na_xTi_{5-x}Zr_xO_{12}$ (x=0, 0.01, 0.03 and 0.05) at 10 C

Fig.8. Nyquist plots of $Li_{4-x}Na_xTi_{5-x}Zr_xO_{12}$ (x=0, 0.01, 0.03 and 0.05)

Fig. 9. The relationship curve between Zre and $\omega^{-1/2}$ in the low frequency

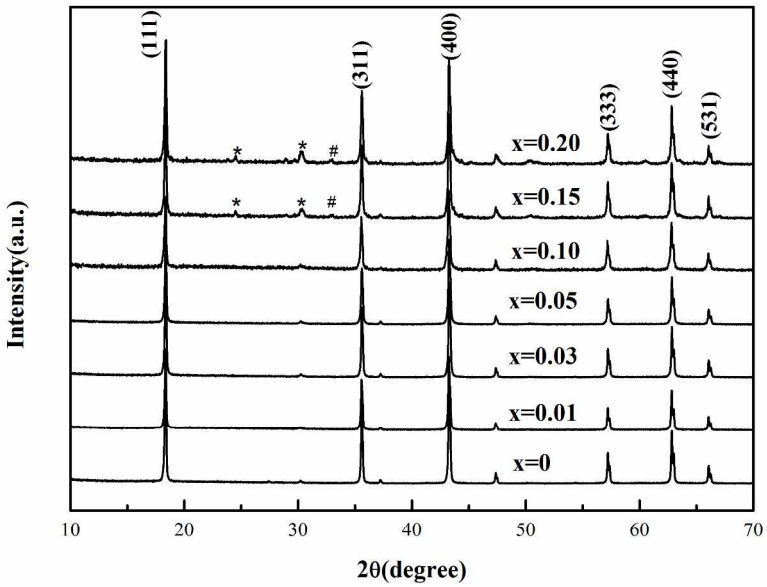

Fig. 1. XRD patterns of as-obtained LTO samples

289x203mm (300 x 300 DPI)

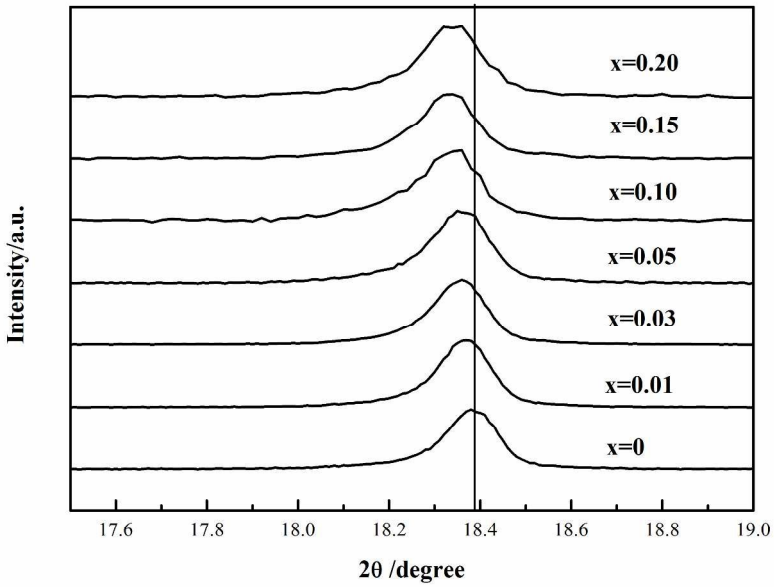

Fig. 2. The enlarged peak of (111) planes of the samples

289x203mm (300 x 300 DPI)

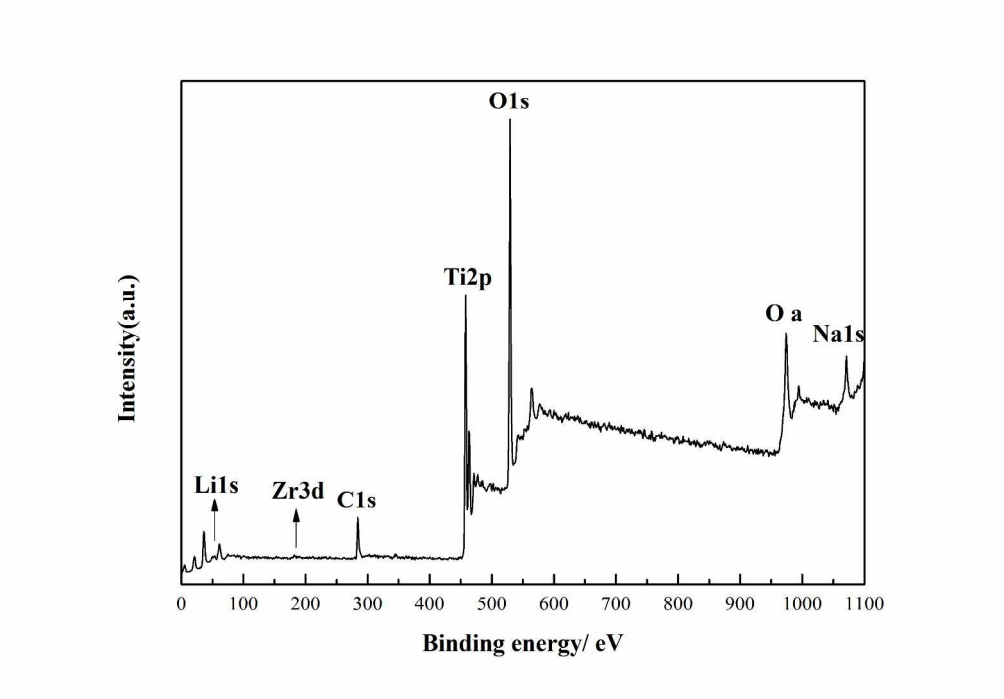

Fig. 3. XPS survey spectra of Li3.97Na0.03Ti4.97Zr0.03O12 (A), typical high-resolution XPS spectra of Na 1s for Li3.97Na0.03Ti4.97Zr0.03O12 (B) and typical high-resolution XPS spectra of Zr 3d for Li3.97Na0.03Ti4.97Zr0.03O12 (C)

289x203mm (300 x 300 DPI)

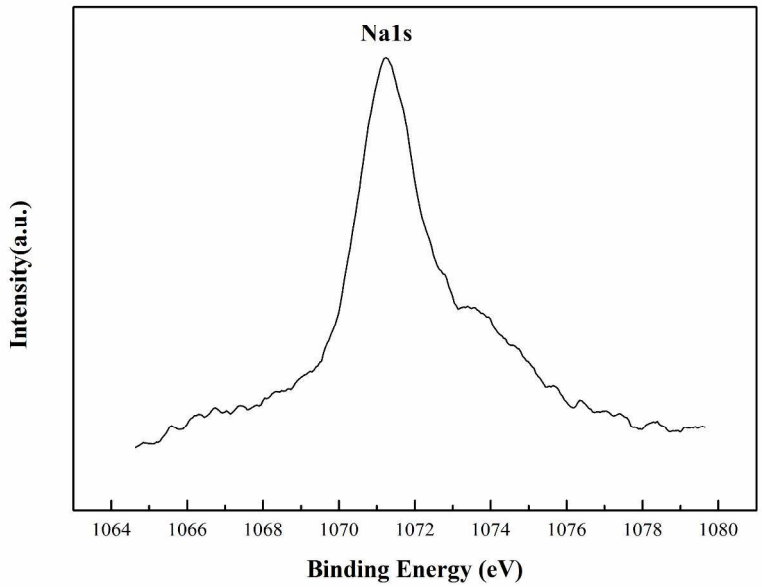

289x203mm (300 x 300 DPI)

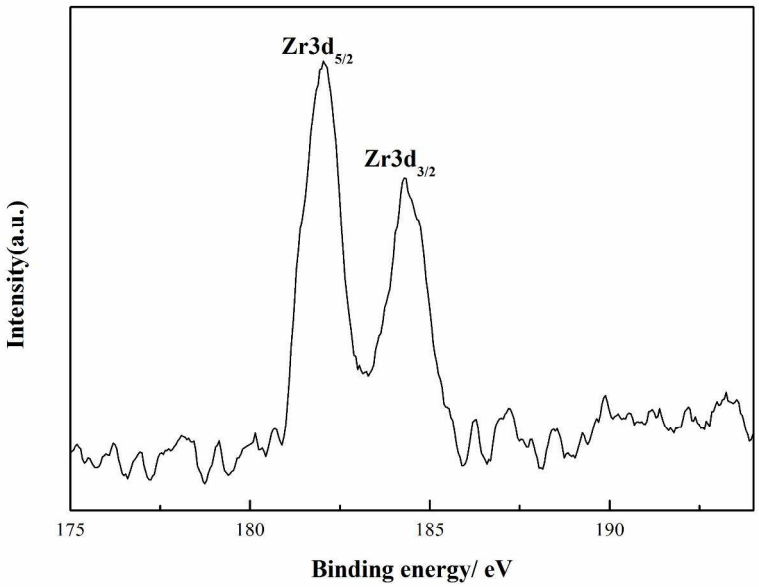

289x203mm (300 x 300 DPI)

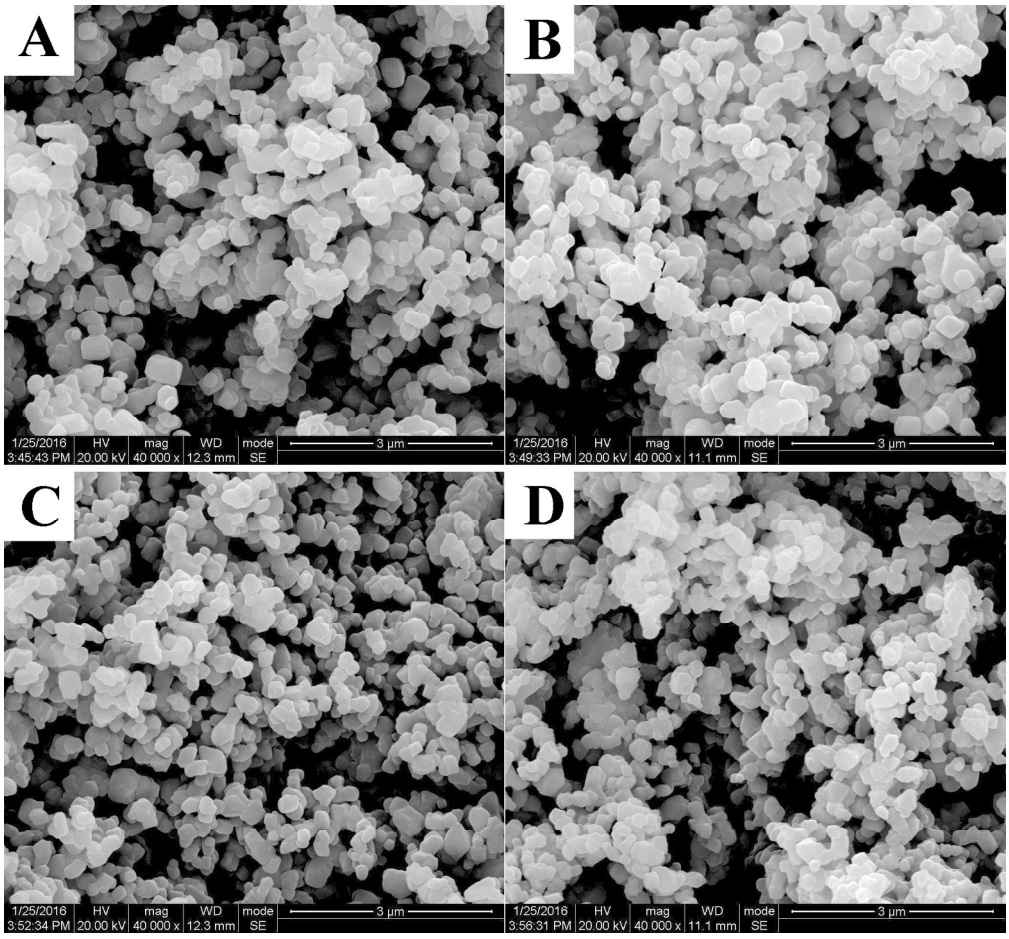

Fig. 4. SEM pictures of Li4−xNaxTi5−xZrxO12 samples: (A) x=0, (B) x=0.01, (C) x=0.03, and (D) x=0.05

723x670mm (72 x 72 DPI)

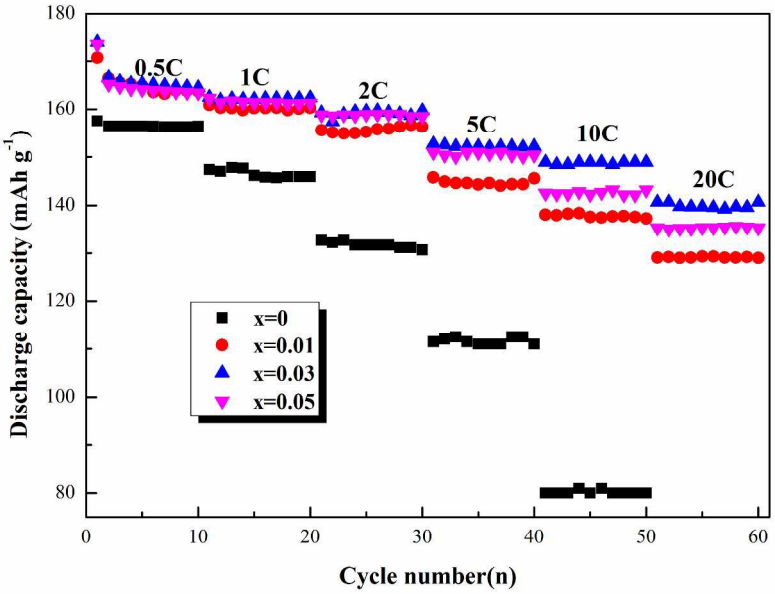

Fig. 5. Cycling performance of Li4−xNaxTi5−xZrxO12 (x=0, 0.01, 0.03 and 0.05) at various rates

289x203mm (300 x 300 DPI)

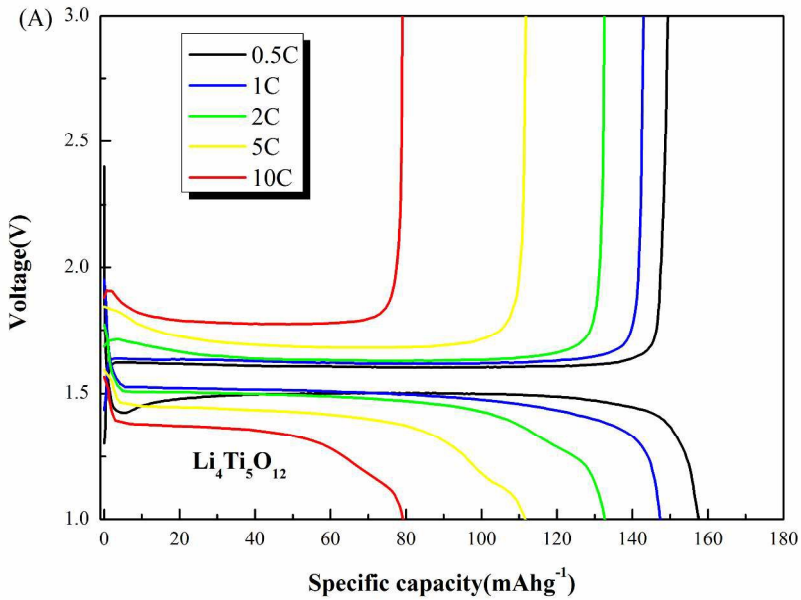

Fig. 6. The first charge and discharge curves for Li4Ti5O12 (A) and Li3.97Na0.03Ti4.97Zr0.03O12 (B) at various rates

289x203mm (300 x 300 DPI)

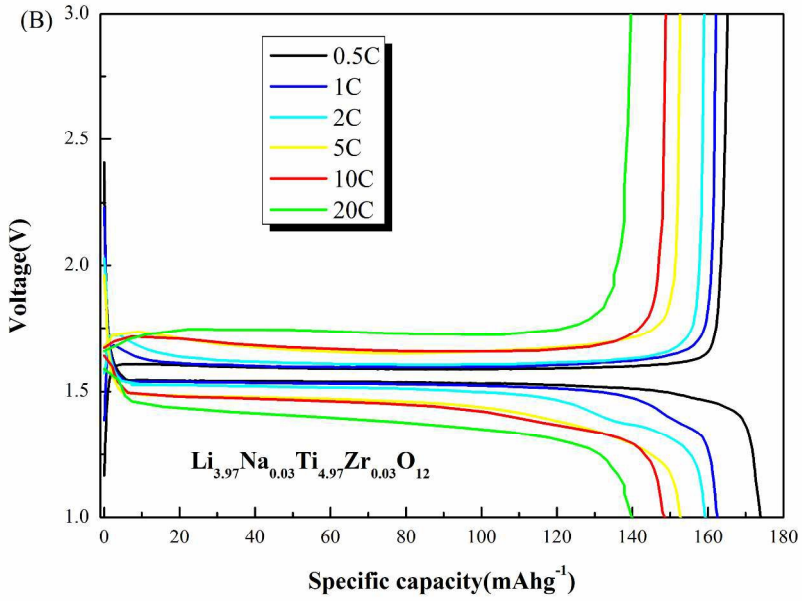

289x203mm (300 x 300 DPI)

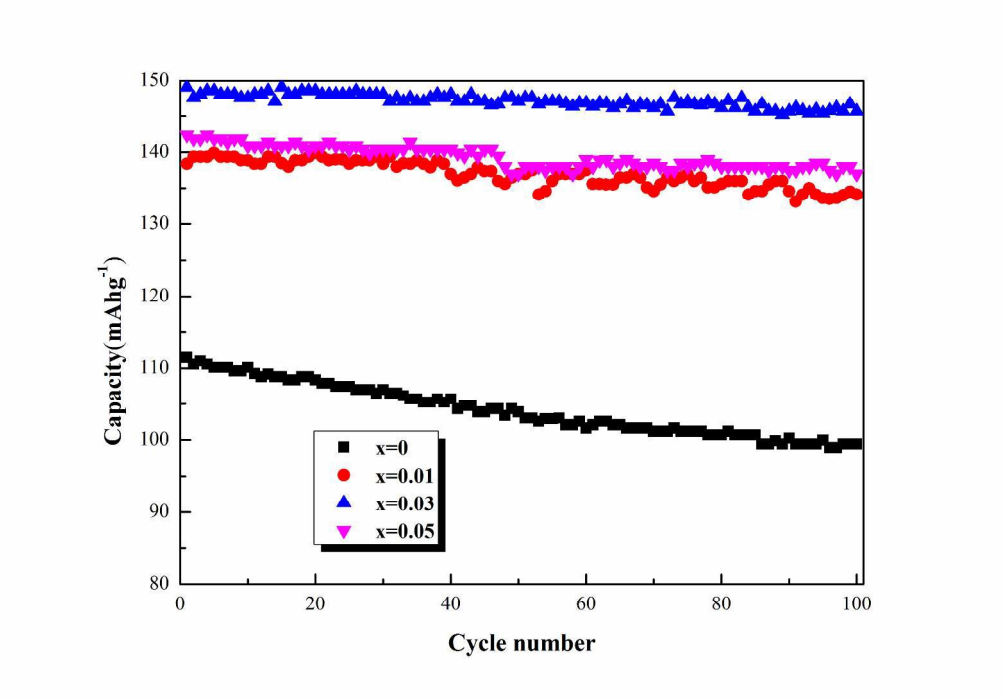

Fig.7. Cyclic performance of Li4−xNaxTi5−xZrxO12 (x=0, 0.01, 0.03 and 0.05) at 10 C

289x203mm (300 x 300 DPI)

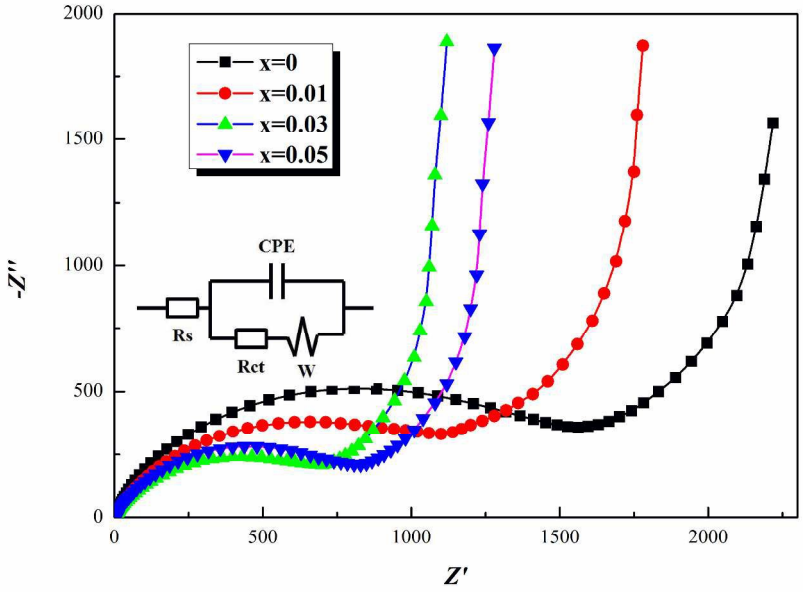

Fig.8. Nyquist plots of Li4−xNaxTi5−xZrxO12 (x=0, 0.01, 0.03 and 0.05)

289x203mm (300 x 300 DPI)

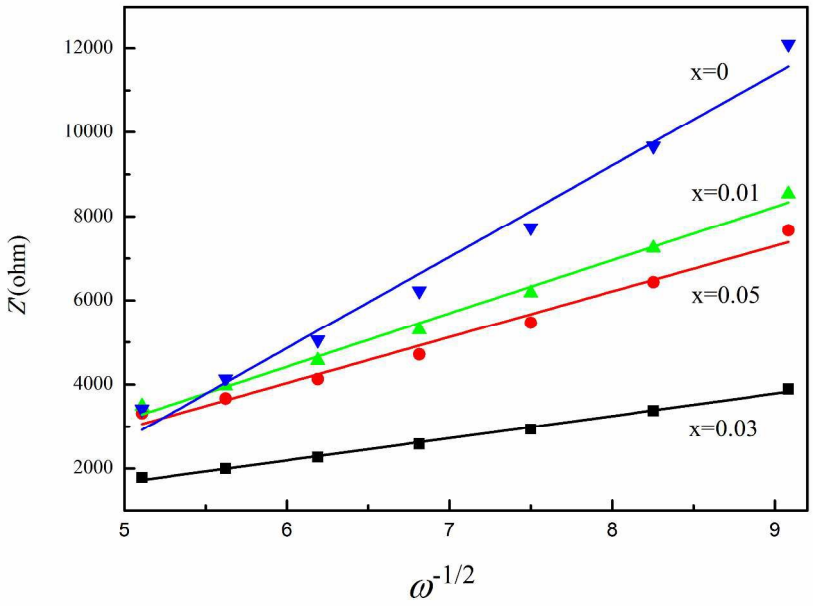

Fig. 9. The relationship curve between Zre and ω−1/2 in the low frequency

289x203mm (300 x 300 DPI)